Geophys. J. Int. (2002) **148,** 663–675

Deterministic non-linear source processes of volcanic tremor signals accompanying the 1996 Vatnajökull eruption, central Iceland

Konstantinos I. Konstantinou*

Dept of Geological Sciences, University of Durham, South Road, Durham DH1 3LE, UK. E-mail: kostas@earth.sinica.edu.tw

Accepted 2001 September 27. Received 2001 September 18; in original form 2000 December 28

SUMMARY

Observations and theoretical considerations have cast doubt on the suggestion that volcanic tremor source processes may be modelled by a linear oscillator that is set into resonance by a sustained disturbance. Volcanic tremor signals that accompanied the 1996 Vatnajökull subglacial eruption, central Iceland, have been analysed using methods from the discipline of non-linear dynamics in order to investigate the possibility that they originated from a non-linear source. The volcano-seismic phenomena associated with the eruption were recorded by a permanent network equipped with broad-band seismometers (HOTSPOT) using a sampling rate of 20 samples s^{-1}. The eruption was preceded by increased seismic activity for a period of 2 days, which also included a large earthquake with a moment magnitude of 5.6. The tremor during the first 2 days of the eruption has a high signal-to-noise ratio at the nearest station to the eruption site and starts as a continuous signal, later evolving to low-amplitude background tremor interrupted by high-amplitude, cigar-shaped bursts having an average duration of 250 s. The phase space, which describes the evolution of the behaviour of a non-linear system, was reconstructed from the original tremor seismograms using the delay embedding theorem suggested by Takens. The delay time used for the reconstruction was selected after examining the autocorrelation function, which showed a first zero crossing at a timelag of 4 samples and the average mutual information that showed no minimum, indicating that the tremor process may have been undersampled. Based also on phase space portraits for different delay times, a delay time of one sample interval (0.05 s) was used. The sufficient embedding dimension for phase space reconstruction was selected by applying the false nearest-neighbours method, which revealed complete unfolding of the tremor attractor at dimensions 7–8, implying upper bounds of its fractal dimension in the range 3.5–4.0. The phase space prediction errors of different segments of the tremor time-series were compared in order to check whether the attractor dynamics change substantially with time. It was found that for continuous tremor there was almost no dynamic variation, in contrast to the background tremor and the superposed bursts that gave a maximum prediction error when the former was used to predict the latter. This difference in dynamics also had an effect on their spectra: the amplitude spectrum of a burst or continuous tremor has a much sharper decay at high frequencies than that of the background tremor. A possible physical mechanism that may explain these observed characteristics involves turbulent slug flow of magma in a narrow cylindrical conduit, generating the different dynamic regimes as the Reynolds number varies.

Key words: non-linear dynamics, turbulent slug flow, Vatnajökull, volcanic tremor.

INTRODUCTION AND BACKGROUND

The identification of a source mechanism that can adequately explain the excitation of volcanic tremor and its observed characteristics remains one of the outstanding problems in the discipline of volcanic seismology. Most source models that have been proposed previously, can be grouped into four broad categories: fluid-flow-induced oscillations of volcanic conduits (Ferrick *et al.* 1982); excitation of fluid-filled cracks (Chouet 1992); hydrothermal boiling in groundwater channels (Leet 1988); oscillation of magma bodies of various geometrical shapes (Kubotera 1974; Chouet 1985; Crosson & Bame 1985). An important ingredient of all of these models is the assumption that the oscillating body (a magma-transporting conduit

*Now at: Institute of Earth Sciences, Academia Sinica, PO Box 1-55, Nankang, Taipei, Taiwan 115, R.O.C.

such as a crack or pipe) behaves as a linear oscillator that may be set into resonance as a result of a sustained disturbance. Resonance and possible path/site effects could also explain the series of sharp spectral peaks observed in many volcanic tremor occurrences (e.g. Ferrazzini & Aki 1992; Goldstein & Chouet 1994).

Observations suggest, however, that tremor source processes exhibit more complexity than any linear model can account for. Fukao *et al.* (1998) reported the occurrence of damped oscillations in volumetric strain records shortly before and after the 1986 Izu–Oshima volcano eruption, Japan, which were followed by volcanic tremor episodes. These oscillations had some unusual characteristics, such as a low-frequency content of either 20 or 40 mHz, with dramatic changes in the polarity of the initial motion. Fukao *et al.* (1998) attributed this behaviour to an episodic supply of magma to the conduit and its subsequent drainage back into the reservoir. They also noted that if this is the disturbance causing the excitation of tremor, then the input forcing frequency they observed is abnormally low in comparison with the resulting high-frequency (1–10 Hz) tremor signal.

On theoretical grounds, Julian (1994) pointed out that the frequency output of a linear oscillator cannot contain frequencies that were not present in its input; therefore a non-linear process of some kind is essential to the ability of a system to generate volcanic tremor. Furthermore, he formulated a lumped-parameter model involving non-linear oscillations excited by the flow of an incompressible viscous fluid through a channel of movable elastic walls. Owing to the Bernoulli effect, whenever the flow speed increases the fluid pressure should decrease and the channel walls will move towards each other to constrict the flow; the opposite process of pressure increase and flow speed decrease will result in the opening of the channel. For increasing values of the pressure parameter there can be a range of types of behaviour, starting with simple cycles of opening and closing of the channel walls exhibiting a harmonic frequency spectrum with sharp peaks, developing to an almost broad-band signal after the fluid pressure exceeds a critical value.

Non-linear oscillations are usually described by ordinary or partial differential equations, which are much more difficult to analyse mathematically than their linear counterparts. One difficulty is that it is impossible to solve such equations analytically, so one must rely heavily on numerical integration and graphical methods of solution representation, in order to have a qualitative view of their behaviour. One such graphical method uses as coordinates the solution x and its time derivatives that appear in the equation $(\dot{x}, \ddot{x}, \ldots, x^{(n)})$ forming an $(n+1)$-dimensional space that is called the phase or state space (Jordan & Smith 1987). The behaviour of the solutions will depend on the initial conditions chosen and on the values of the free parameters present in the equations. Possible drifting in the values of these parameters is going to cause a change in the qualitative character of the solutions, a phenomenon that is defined as bifurcation (Drazin 1994). After some parameter has reached a critical value, owing to a series of repeated bifurcations the solution will move to an aperiodic and almost random-looking regime, which Li & York (1975) called chaos.

Lorenz (1963) first demonstrated the existence of chaotic solutions by solving numerically a set of three coupled non-linear differential equations, which represented a simplified version of the Navier–Stokes equations in fluid dynamics. He also showed that the solutions, when plotted in the phase space, defined orbits that were attracted to a specific region and were unable to escape from it. The geometrical object that was formed in the phase space, had a fractal structure and a non-integer dimension, therefore it was later called a 'strange' attractor (Ruelle & Takens 1971). Since Lorenz's discovery, systems governed by non-linear differential equations that may also have chaotic solutions were found to exist in almost every scientific discipline. Geophysical examples of such systems include the vertical ground movements in the Campi Flegrei caldera (Cortini *et al.* 1991), rays that propagate through strongly laterally varying media (Keers *et al.* 1997) and variations in the period of rotation of the Earth (Frede & Mazzega 1999).

This work aims to investigate the possibility put forward by the arguments presented above, that volcanic tremor signals may be the result of non-linear processes for the case of tremor data recorded during the 1996 Vatnajökull eruption in central Iceland. This task is accomplished using a variety of methods of non-linear time-series analysis based on the theory of non-linear dynamics. First, a brief summary of the seismicity associated with the eruption is presented, placing emphasis on the temporal evolution of the tremor behaviour. Next, the problem of phase space reconstruction from the vertical component seismogram records is considered, in an attempt to recover the attractor that controls the generation of tremor. Taking advantage of the fact that the future states of a non-linear system can be predicted in the phase space, prediction errors of different segments of the tremor time-series are compared, in order to determine whether the attractor dynamics change substantially in time. Finally, the results of this analysis are discussed and compared with those obtained by a similar study on Hawaiian tremor, published by Chouet & Shaw (1991).

DESCRIPTION OF THE 1996 VATNAJÖKULL ERUPTION

The Vatnajökull glacier is a permanent ice cap that covers a large part of central Iceland (Fig. 1). Underneath this ice cap a number of central volcanoes exist and the most active of them, situated at its NW part, are Bárdarbunga and Grimsvötn. Only during the last century six major eruptions have occurred in the area, producing volumes of erupted lava that range from 0.03 to 0.4 km^3 (Gudmundsson & Björnsson 1991). A consequence of the interaction of magma with ice is the production of large amounts of meltwater that are usually drained underneath the glacier to the south coast, causing catastrophic floods.

A detailed description of the main phase of the eruption, including the event location procedure used, the classification of the volcanic earthquakes and spectral analysis of tremor, has been published elsewhere (Konstantinou *et al.* 2000) therefore only a brief summary will be given here. The seismicity associated with the 1996 eruption started at 10:45 GMT, September 29 with an $M_w = 5.6$ earthquake occurring in the area of the Bárdarbunga caldera (Einarsson *et al.* 1997). Focal mechanisms of this earthquake obtained by waveform inversion of teleseismic data indicate a substantial non-double-couple component that can be interpreted either as a rupture along a ring fault (Nettles & Ekström 1998) or breaking of an asperity (Zobin 1999) caused by an inflating magma chamber underneath Bárdarbunga. About half an hour later an episodic swarm of low-frequency earthquakes (1–2 Hz) followed, with epicentres that delineated the rim of the Bárdarbunga caldera. In the afternoon the seismic activity declined but resumed again during the evening with a swarm of mixed-frequency events (1–4 Hz) migrating towards Grimsvötn. During the following 2 days (September 30–October 1) the onset of the subglacial eruption took place, with mixed-frequency events occurring in the area between the two volcanoes. The eruption became subaerial on the afternoon of October 2 and an eruption fissure was formed, while the seismic

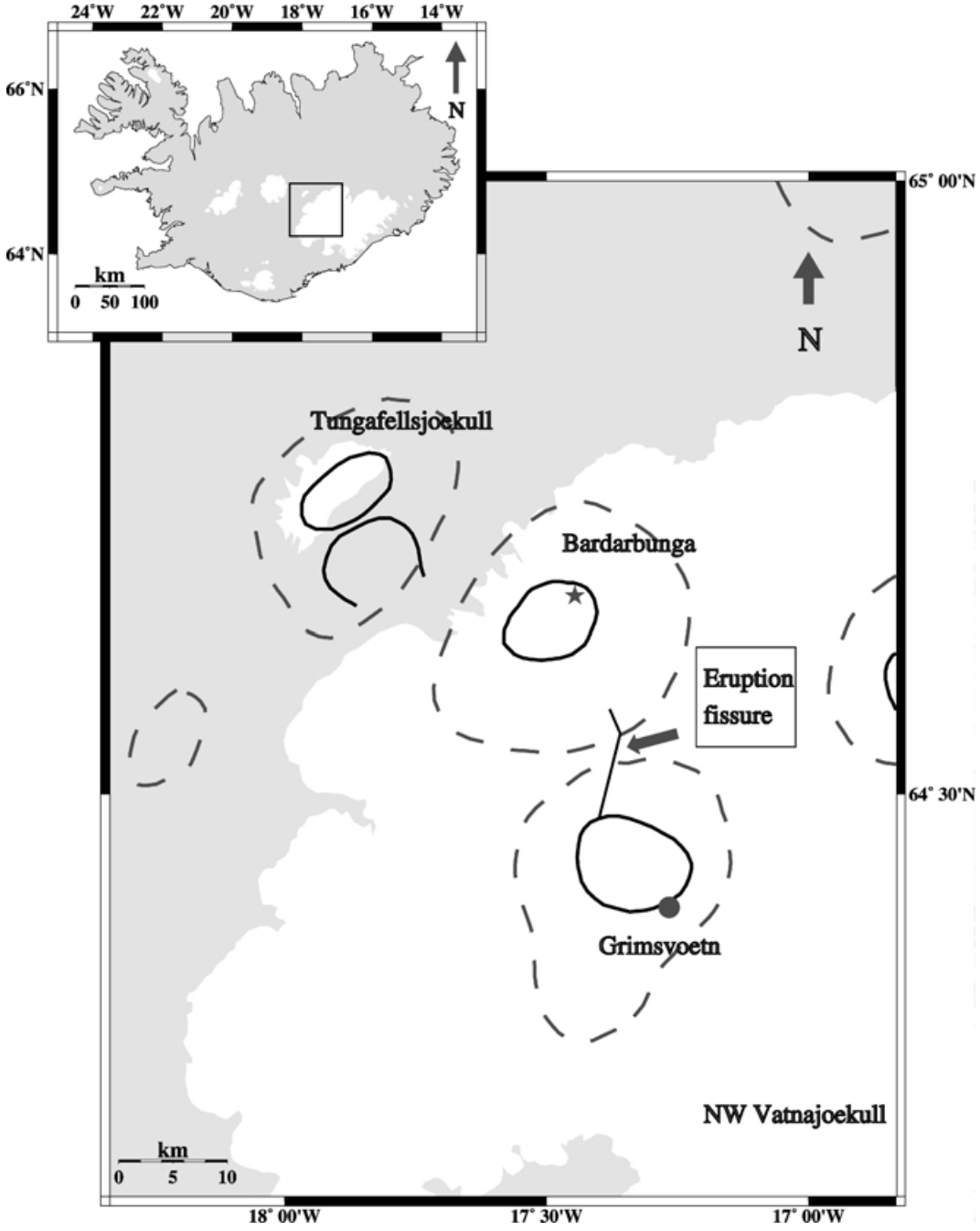

Figure 1. The NW part of the Vatnajökull glacier where the 1996 eruption took place (unshaded terrain is ice covered). Solid lines represent the outline of calderas and dashed lines the outlines of central volcanoes. The epicentre of the $M_w = 5.6$ Bárdarbunga earthquake that initiated the seismic activity is shown by the star. The black dot indicates the position of the closest station, HOT23. The inset shows the relative location of the eruption site on the map of Iceland (white areas indicate permanent glaciers).

activity started to decline. In the following days (October 3–6) only a few earthquakes occurred near the fissure, while most of the activity consisted of low-frequency events and had shifted northwards to the area between the Bárdarbunga and Tungafellsjökull volcanic systems.

All volcano-seismic phenomena related to the eruption were recorded using temporary (HOTSPOT) and permanent (SIL) seismic networks, covering most parts of the country (Fig. 2). HOTSPOT was a joint project between Princeton and Durham Universities, the Icelandic Meteorological Office and the US Geological Survey, having as its primary purpose the collection of high-quality digital data of local and teleseismic events. HOTSPOT consisted of 30 stations equipped with broad-band three-component instruments, that had a flat velocity response in the frequency range 0.03–20 Hz and Refraction Technology 72a-02 16-bit data loggers recording continuously at a rate of 20 samples s^{-1}, while absolute timing was provided by GPS receivers. HOTSPOT remained in operation for the 2-year period between 1996 August and 1998 August. The South Iceland Lowlands (SIL) network is operated by the Icelandic Meteorological Office and consisted (at the time of the eruption)

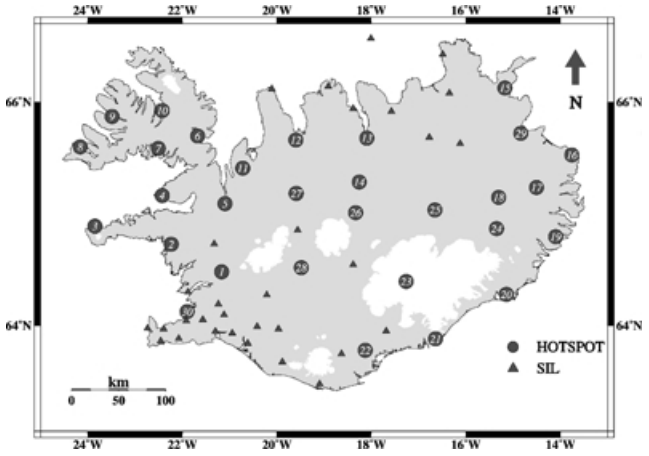

Figure 2. Map showing the location of the temporary (HOTSPOT) and permanent (SIL) networks that were operational during the Vatnajökull eruption.

of 30 stations with broad-band or short-period sensors, recording local earthquake data using a triggering mechanism at a rate of 100 samples s^{-1}.

During September 28–29 the seismograms recorded at the closest station to the eruption site (HOT23) were severely contaminated by ocean microseismic noise (Fig. 3) with a dominant frequency of 0.25 Hz. No other seismic signal was visible, however, examination of the frequency domain during that period by means of spectrograms showed the existence of a higher-frequency signal in five narrow bands (0.5–0.7, 1.6, 2.2, 2.8, 3.2 Hz) (Konstantinou *et al.* 2000). In the days that followed volcanic tremor became broad-band, but isolated peaks at almost the same frequency bands could still be distinguished in the spectrograms. An attempt to recognize particular wave types was not successful, since it was found that the tremor wavefield was composed of a complex mixture of body and surface waves; similar observations have been published for tremor from the Arenal volcano in Costa Rica (Hagerty *et al.* 2000) and Mt Semeru in Indonesia (Schlindwein *et al.* 1995).

Tremor activity started being visible on the seismograms at the onset of the eruption as a relatively low-amplitude, continuous signal just above the level of ocean microseismic noise (Fig. 4). During the night of October 1 the amplitude of the signal increased progressively, being visible at HOT23 without having to perform any filtering. Similar activity continued until midday when high-amplitude, cigar-shaped bursts started being superposed on the lower-amplitude background tremor (Fig. 5). The number of bursts steadily declined as the eruption was progressing (Fig. 6a), while their average duration was of the order of ± 250 s with a standard deviation that varied considerably from day to day (Fig. 6b). After the eruption became subaerial there were episodic cycles of high-amplitude tremor mixed with periods when only ocean microseismic noise could be seen. Spectrograms of the data recorded on October 13 do not show the presence of any higher-frequency signal, thus marking the end of the tremor activity.

RECONSTRUCTION OF THE PHASE SPACE

The problem of reconstruction of the phase space from a scalar time-series (such as a seismogram) is of great practical importance, since it is the starting point of all non-linear time-series analysis methods. Any time-series resulting from a non-linear process can be considered as the projection on the real axis of a higher-dimensional geometrical object that describes the behaviour of the system under study (Kantz & Schreiber 1996). Takens (1981) and later Sauer *et al.* (1991), showed that it is possible to recover this object from a series of scalar measurements $s(t)$ in an m-dimensional Euclidean space using points $\mathbf{y}$ with coordinates

$$\mathbf{y} = s(t), s(t+\tau), \ldots, s(t+(m-1)\tau), \tag{1}$$

where τ is called the delay time and for a digitized time-series is a multiple of the sampling interval used. The dimension m of the reconstructed space is considered as the sufficient dimension for recovering the object without distorting any of its topological properties, thus it may be different from the true dimension of the space where this object lies. This procedure of phase space reconstruction is termed embedding and the formulation of Takens is called the delay embedding theorem, with m being the embedding dimension. In practical applications both the delay time and the embedding dimension have to be determined from the time-series itself.

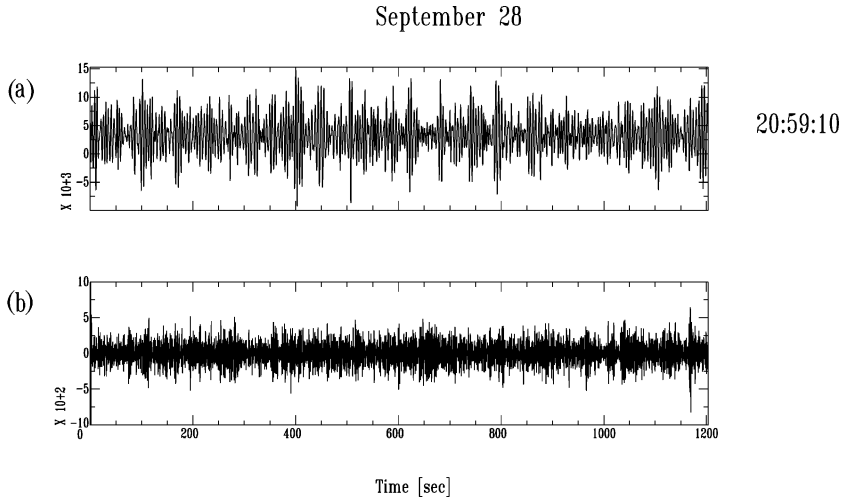

Figure 3. (a) Vertical component velocity waveform recorded at HOT23 2 days before the onset of the eruption showing contamination with microseismic noise. (b) The same trace after high-pass filtering at 0.5 Hz, revealing a low-amplitude high-frequency signal. The spectrograms for this time period exhibit peaks at 0.5–0.7, 1.6, 2.2, 2.8 and 3.2 Hz. The time given on the right is the start time (GMT) for the trace.

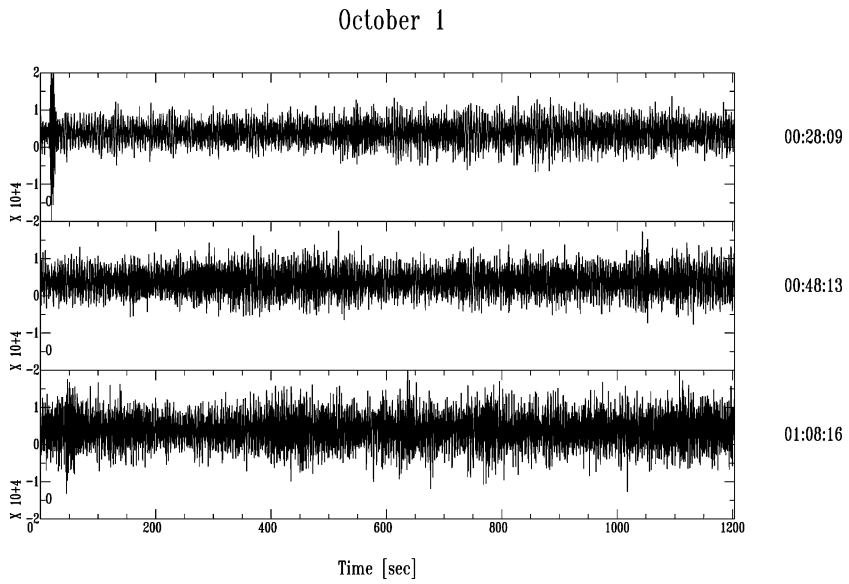

Figure 4. One hour of continuous volcanic tremor during the onset of the subglacial eruption recorded at HOT23. The times given on the right are the start times (GMT) for each trace. The amplitude scale is normalized to the largest value of the three traces (last trace). The large-amplitude signal at the beginning of the first trace is an earthquake. Note the gradual increase of the tremor amplitude.

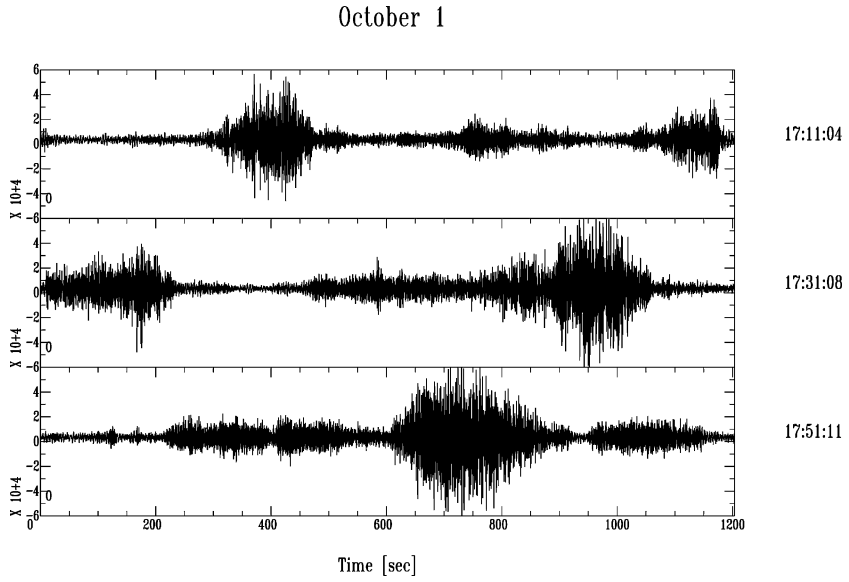

Figure 5. Same as in Fig. 4 for tremor exhibiting high-amplitude, cigar-shaped bursts that are superposed on low-amplitude background tremor. Note how some of the bursts have a slow amplitude decay while others decay abruptly.

In the case of the tremor signals that were recorded during the 1996 Vatnajökull eruption a selection of suitable data for the reconstruction of the phase space had to be made. The main criterion for suitability concerns the amount of contamination of the data by ocean microseismic (or possibly other) noise. Earlier studies have revealed that filtering the data in order to remove the noisy part of the signal may result in a change in the original number of degrees of freedom (and therefore of the embedding dimension) of the system (Brandstätter & Swinney 1987; Abarbanel *et al.* 1993). In this study only data recorded at the nearest station to the eruption site (HOT23) are considered, where a tremor could be clearly seen with a high signal-to-noise ratio during the first 2 days of the eruption (October 1–2).

Selection of the delay time

One proposed way of choosing the delay time τ for phase space reconstruction is by calculating the autocorrelation function of the data and choosing τ as the time of the first zero crossing (e.g. Kantz & Schreiber 1996). A characteristic of chaotic time-series is that their autocorrelation functions drop to zero very quickly, reflecting the fact that the past states of the system decorrelate exponentially from the future ones. By calculating the autocorrelation function of the tremor data for timelags of 0–40 samples (2 s) it was found that in most cases the first zero crossing was reached very quickly at a delay time of four samples (0.2 s) (Figs 7a and b). An objection to the selection of the delay time in this way is that the autocorrelation

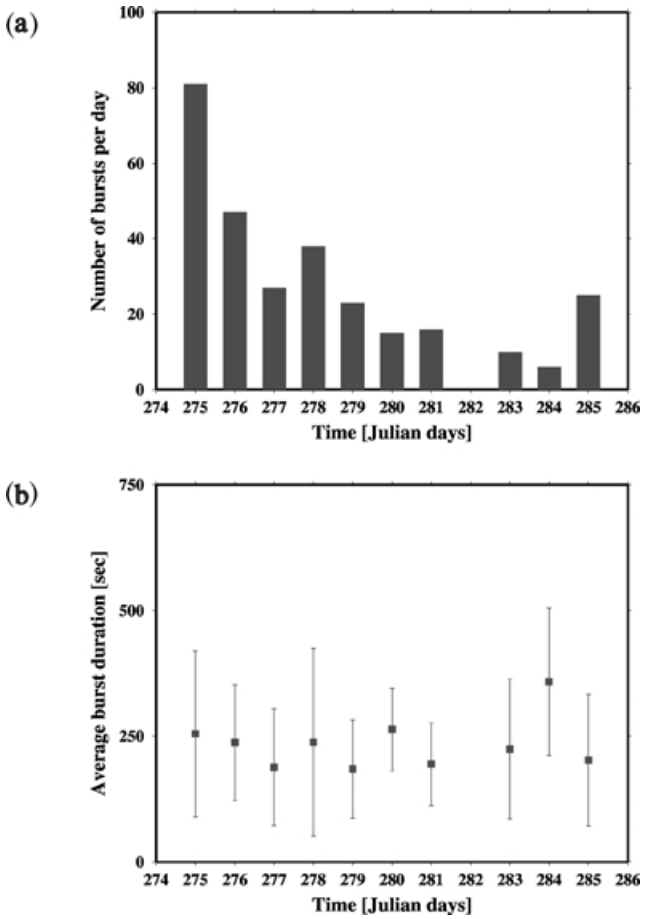

Figure 6. (a) Distribution of the number of bursts during the whole period of the eruption (October 1–11). (b) Average duration and standard deviation of the bursts for each day.

function takes into account only linear correlations of the data (Abarbanel 1996). Fraser & Swinney (1986) proposed a kind of non-linear autocorrelation function for time delay selection, which they called average mutual information (AMI) defined as

$$I(\tau) = \sum_{ij} p_{ij}(\tau) \ln p_{ij}(\tau) - 2 \sum_{i} p_i(\tau), \tag{2}$$

where p_i is the probability that the signal $s(t)$ assumes a value inside the ith bin of a histogram, while p_{ij} is the probability that $s(t)$ is in bin i and $s(t+\tau)$ is in bin j. When τ becomes large, then $s(t+\tau)$ conveys no information concerning $s(t)$ and p_{ij} factorizes to $p_i p_j$ yielding $I(\tau) = 0$.

Based on the fact that the first minimum of AMI marks the delay time where $s(t+\tau)$ adds maximum information to the knowledge we have from $s(t)$ (or where the redundancy is the least), this time is considered to be the best choice for τ. AMI was calculated for the data for timelags of 0–100 samples (5 s) and for time windows of 5, 10, 20 min, having very small variation and showing no minimum in each case (Figs 7c and d). The absence of a minimum from the AMI graph usually indicates that the data have not been sufficiently sampled, in which case a delay time of $\tau = 1$ sample (0.05 s) is considered the most suitable choice (Abarbanel 1996). A consequence of undersampling is that it precludes the application to the data of any method for the calculation of fractal dimensions or Lyapunov exponents, which both require well-resolved phase space orbits in order to give reliable results.

In order to make a final decision concerning the value of the delay time, 2-D phase portraits of the tremor attractor were reconstructed using delay times in the range of one to four samples (0.05–0.2 s) (Fig. 8). A value of τ smaller than the optimum will result in the clustering of the points along the diagonal of the phase portrait, while a value greater than the optimum would make the attractor take a complicated shape. The latter case occurs at delay times with three to four samples (0.15–0.2 s) as demonstrated by the phase portraits in Figs 8(c) and (d). For delay times of one to two samples (0.05–0.1 s) the points are spread over the two sides of the diagonal and are not tightly clustered along it. Taking into account the indication of undersampling obtained using the AMI method, it is concluded that the best choice of the delay time is $\tau = 1$ sample (0.05 s).

Selection of the embedding dimension

The selection of a sufficient dimension that can be used for the embedding relies on the principle that orbits of attractors describing non-periodic signals should not intersect (e.g. Abarbanel 1996). Any intersection means that the orbit is revisiting exactly the same parts of the phase space, which implies periodic rather than chaotic behaviour. This kind of intersection or overlap between orbits results when the attractor is embedded in a dimension lower than the sufficient one stated by the embedding theorem. If two points $\mathbf{y}^a$ and $\mathbf{y}^b$ are close in the same neighbourhood in phase space, this is so either because the dynamic evolution of the orbits brought them close or owing to an overlap resulting from the projection of the attractor to a lower dimension. In order to decide which of the two possibilities is true, a comparison should be made of the Euclidean distance of the two points $|\mathbf{y}^a - \mathbf{y}^b|$ in two consecutive embedding dimensions d and $d+1$. For an embedding dimension m and delay time τ these distances are given by (Kennel *et al.* 1992)

$$R_d^2 = \sum_{m=0}^{d-1} [s^a(t+m\tau) - s^b(t+m\tau)]^2 \tag{3}$$

moving from dimension d to $d+1$ means that a new coordinate is being added in each delay vector, which is equal to $s(t+d\tau)$. The Euclidean distance of the two points in dimension $d+1$ will thus be

$$R_{d+1}^2 = R_d^2(t) + |s^a(t+d\tau) - s^b(t+d\tau)|^2. \tag{4}$$

The relative distance between the two points in dimensions d and $d+1$ will then be the ratio

$$\sqrt{\frac{R_{d+1}^2 - R_d^2}{R_d^2}} = \frac{|s^a(t+d\tau) - s^b(t+d\tau)|}{R_d}. \tag{5}$$

If this distance ratio is greater than a predefined value, say v, then the points $\mathbf{y}^a$ and $\mathbf{y}^b$ are characterized as 'false' neighbours, being in the same neighbourhood because of the projection and not because of the dynamics. The procedure is repeated for all pairs of points at higher dimensions until the percentage of false neighbours becomes zero and then the attractor is said to be unfolded. For limited data sets, Kennel *et al.* (1992) found it necessary to add a second criterion for characterizing two points as false neighbours, which is

$$R_{d+1} > \frac{\sigma}{v}, \tag{6}$$

where σ is the standard deviation of the data around its mean. Taking σ as a representative measure of the size of the attractor, this criterion reflects the fact that if two points are false neighbours, they will be

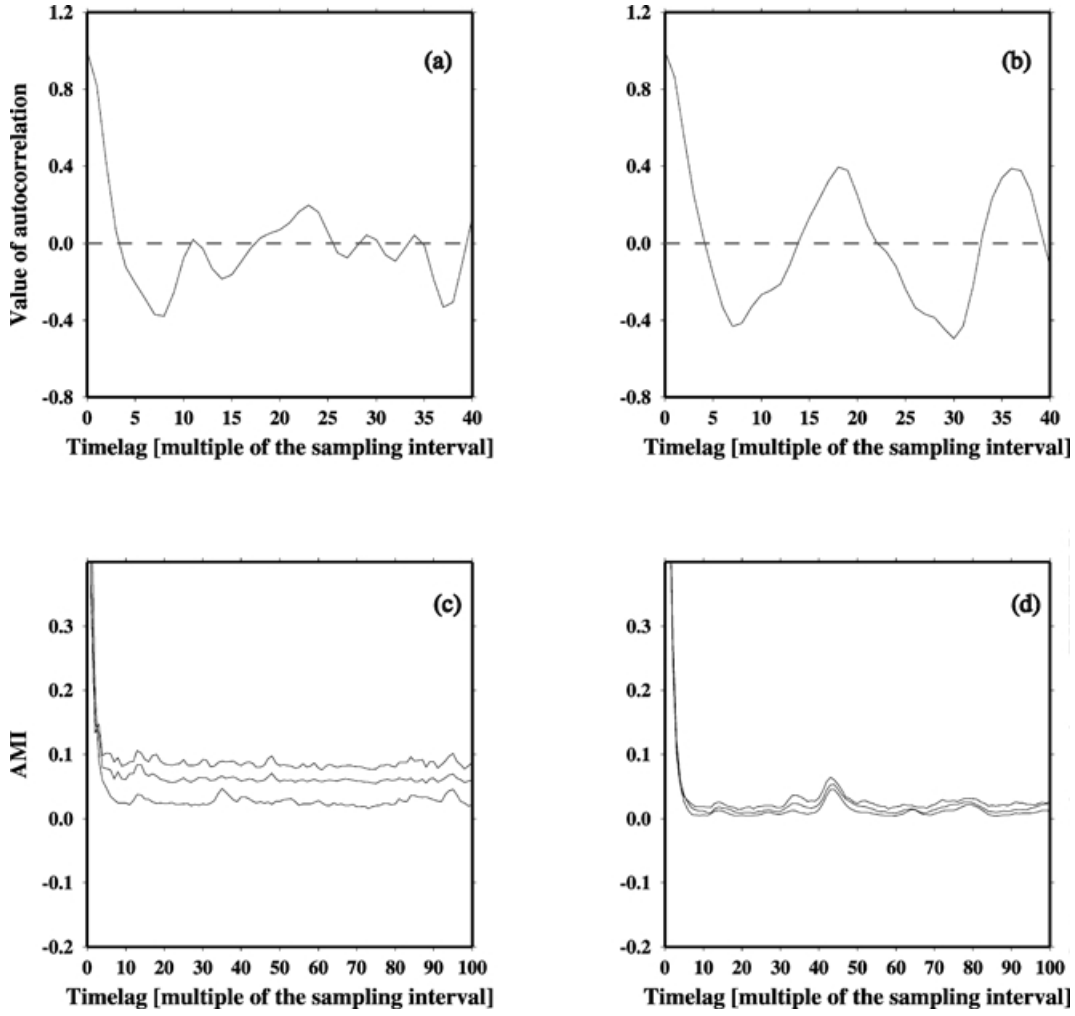

Figure 7. Top panel: autocorrelation function calculated for a 5 min window of (a) high-amplitude burst and (b) continuous tremor. Lower panel: average mutual information calculated for delay times 1–100 using 5, 10 and 20 min of data for (c) a data segment that contains a high-amplitude burst and (d) continuous tremor (the small peak in each of the three AMI estimates probably represents a random fluctuation of AMI in the data).

stretched to the extremities of the attractor when they are unfolded from each other at dimension $d + 1$. The authors also noted that a false nearest-neighbours algorithm that does not implement this criterion will give an erroneous low embedding dimension even for high-dimensional stochastic processes.

Naturally, two important issues that have to be addressed concern the length of the analysis window that should be used and the selection of a suitable value for v. The length of the analysis window is usually chosen in such a way that the points resulting from the embedding populate the attractor as densely as possible. However, the long duration of the tremor data poses a trade-off between large windows, which would also include more noise and need extra computer time for each analysis, while in that time interval the properties of the source may vary substantially; on the other hand, smaller windows may give biased false-neighbour statistics. Since the time-series length used in similar studies was usually in the range of 10 000–32 000 samples (e.g. Brandstätter & Swinney 1987; Frede & Mazzega 1999), the analysis of the tremor data was conducted using segments with a duration of 20 min (24 000 samples). The value to which the distance ratio of the points is compared has been found for many non-linear systems by Abarbanel (1996) to be around 15. Values in the range of 1–20 were tested in order to see what effect this variation may have on the distribution of the false nearest-neighbour statistics in dimensions 1–10. Most of the data show a 0 per cent false neighbours at either dimension seven or eight for $v = 9$–17 (Fig. 9). Knowing the exact embedding dimension m of the attractor makes it possible to estimate upper bounds for its fractal dimension D_F, since according to the embedding theorem $m > 2D_F$, thus in our case the upper values of D_F are between 3.5 and 4.0.

The percentage of false neighbours did not drop to zero for a number of time segments that were recorded in the early hours of October 1 (01:48–07:10 GMT) implying the presence of random noise in the data (Fig. 10). As a stochastic process, noise should have infinite degrees of freedom, showing no tendency to unfold at any specific dimension. Non-linear deterministic signals that are contaminated by noise usually show a non-zero percentage of false neighbours even at high dimensions. This effect can be easily demonstrated by adding different amounts of random noise to a data segment that otherwise has 0 per cent false neighbours at dimension eight (Fig. 11). A possible explanation for the presence of a random noise source in that time interval is the interaction of rising magma with ice and the subsequent flash boiling that took place. The fact that this noise source disappears later may be attributed

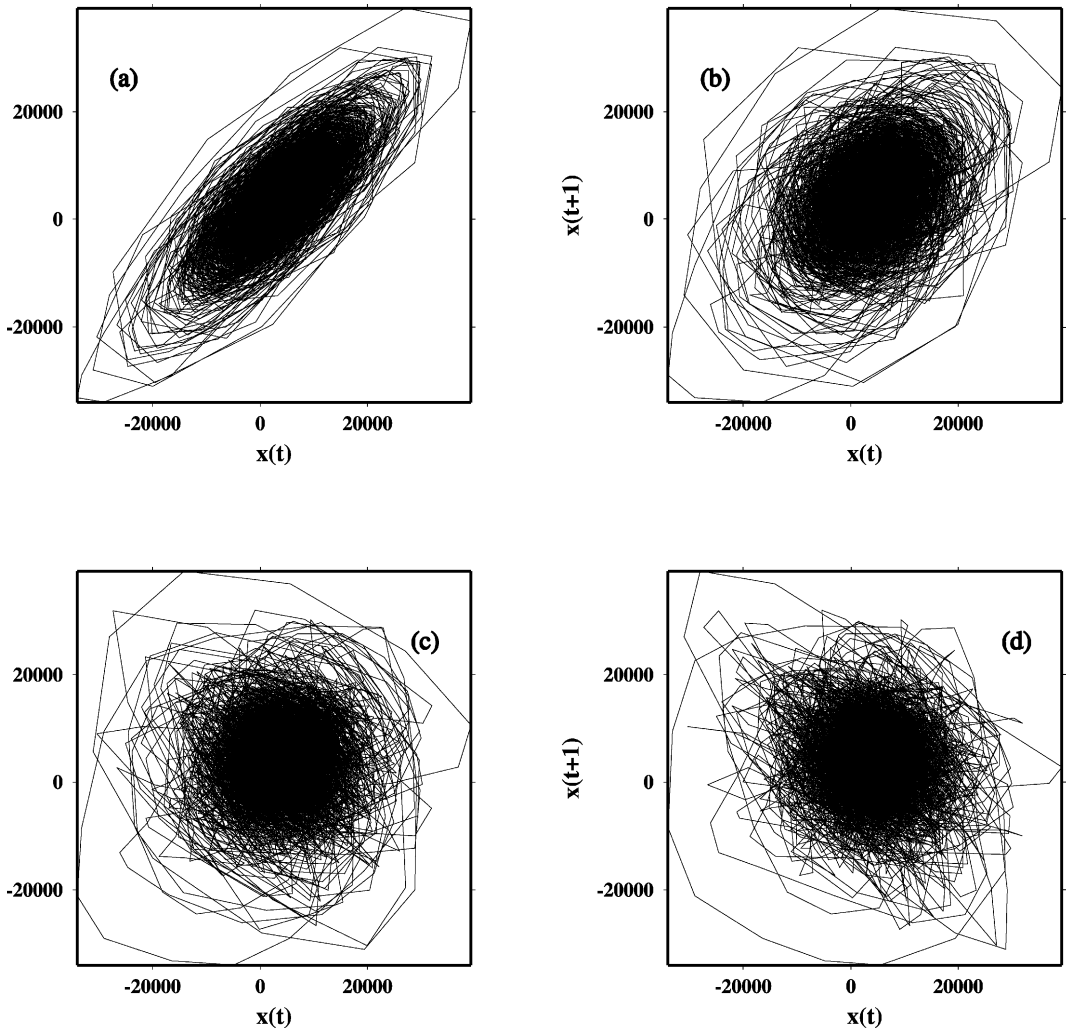

Figure 8. 2-D phase portraits of the tremor attractor, reconstructed using 20 min of data (24 000 samples) and delay time (a) $\tau = 1$ (0.05 s), (b) $\tau = 2$ (0.1 s), (c) $\tau = 3$ (0.15 s) and (d) $\tau = 4$ (0.2 s).

to two factors: first, the ice-melting and boiling process has moved from the rock–ice interface upwards, entirely into the ice cap and second, the flanks of the magma–ice interface should have cooled rapidly and solidified as pyroclastic glass with a temperature of 0 °C (Gudmundsson *et al.* 1997), precluding any further boiling. Taking into account that the sensor of station HOT23 was installed on a rock outcrop and not on ice makes this explanation quite plausible.

TEMPORAL VARIATIONS OF PHASE SPACE DYNAMICS

The cross-prediction method

Changes in the dynamics of the orbits in the phase space usually represent variations of the physical parameters that control a non-linear system and consequently are of great importance for any modelling effort. Since in most cases the only available data are a time-series, monitoring the temporal changes in the dynamics is the most appropriate way of detecting different dynamic regimes in a signal. One method of doing this is to divide the time-series into segments and for each segment to calculate a quantity (the fractal dimension, Lyapunov exponents, etc.) relevant to the dynamics, mapping in effect its variation as a function of time. Two problems regarding this approach are: (1) the choice of an appropriate quantity, bearing in mind that the fractal dimension and Lyapunov exponents need very well-resolved orbits and noise levels of lower than 2 per cent (Kantz & Schreiber 1996) in order to yield meaningful results, and (2) how measurements from different segments can be compared directly instead of just estimating their statistical properties.

Schreiber (1997) proposed a method that utilizes the direct comparison of prediction errors between different parts of a given time-series. Based on the assumption that the signal is a deterministic one, then after reconstructing the phase space using delay vectors $\mathbf{y}_1, \mathbf{y}_2, \ldots, \mathbf{y}_N$ the dynamics may be approximated by the difference equation

$$\mathbf{y}_{n+1} = \mathbf{F}(\mathbf{y}_n). \tag{7}$$

Knowing the present state of the system $\mathbf{y}_n$ it is possible to predict one step into the future $\mathbf{y}_{n+1}$ in the following way: since the function $\mathbf{F}$ describing the evolution of the dynamics is continuous, a past state $\mathbf{y}_{n'}$ very close to the present one is taken and its image $\mathbf{y}_{n'+1}$ is used as the predicted future value. However, when using such a prediction scheme two issues should be taken into account: (a) predictions will become exponentially inaccurate as one tries to predict more

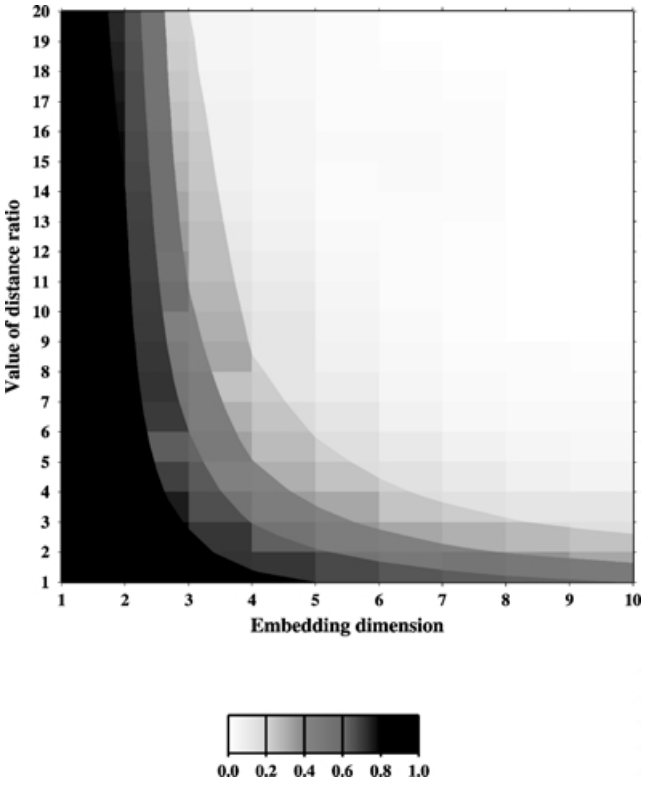

Figure 9. Distribution of the fraction of false nearest neighbours (represented by the grey-scale) as a function of the value of distance ratio for embedding dimensions 1–10 (see text for more details).

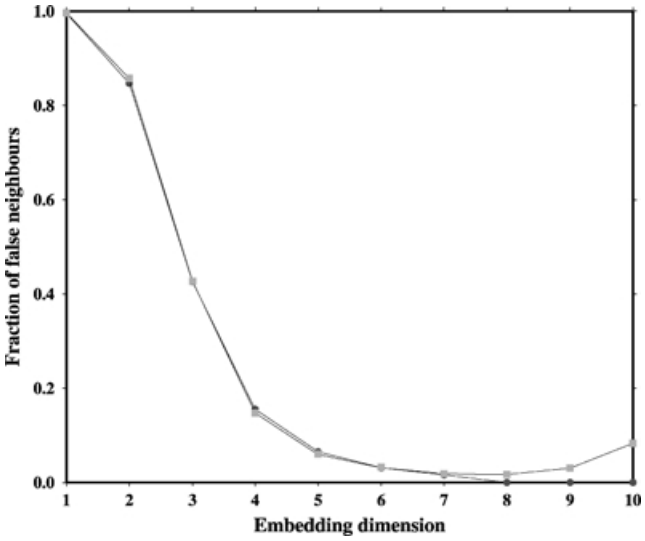

Figure 10. Distribution of the fraction of false nearest neighbours calculated for a data segment recorded on October 1 at 00:28 GMT (black circles) and at 05:08 GMT on the same day (grey squares) for $v = 10$, showing a non-zero percentage of false neighbours in dimensions 1–10 for the latter.

than one step into the future, and (b) since all interpoint distances are contaminated with an uncertainty owing to the finite resolution of the data, all points closer than a distance ϵ are equally good for predicting $\mathbf{y}_{n+1}$. By forming a neighbourhood $\mathcal{U}_{(y_{n'})}$ of radius ϵ around $\mathbf{y}_n$, the final predicted value $\hat{\mathbf{y}}_{n+1}$ will be the arithmetic mean of all the images $\mathbf{y}_{n'+1}$,

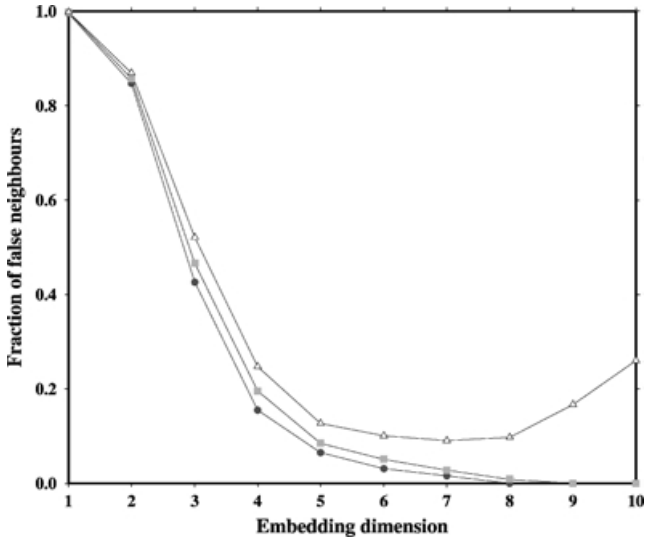

Figure 11. The effect of different amounts of random noise on the false nearest-neighbour statistics for $v = 10$. Black circles indicate the original data, grey squares and white triangles indicate the same data with the addition of 5 and 10 per cent of random noise, respectively.

$$\hat{\mathbf{y}}_{n+1} = \frac{1}{\left|\mathcal{U}_{(y_{n'})}\right|} \sum \mathbf{y}_{n'+1}, \tag{8}$$

where $|\mathcal{U}_{(y_{n'})}|$ is the number of points in the neighbourhood $\mathcal{U}_{(y_{n'})}$. This method of prediction was first suggested by Lorenz (1969) and was later used by Kennel & Isabelle (1992) for detecting deterministic structure in real data sets.

In order to compare the prediction errors of different parts of a time-series, it is split into a number of non-overlapping segments of equal length. If the prediction is performed inside segment i, then the resulting predicted value is going to be $\hat{\mathbf{y}}^i_{n+1}$. Instead of comparing it with the actual value $\mathbf{y}_{n+1}$ in that segment, it is compared with its equivalent in segment j, and the root mean squared prediction error $\gamma(i, j)$ is defined as (Schreiber 1997)

$$\gamma(i, j) = \sqrt{\frac{1}{N} \sum_{n=0}^{N-1} \left(\hat{\mathbf{y}}^i_{n+1} - \mathbf{y}^j_{n+1}\right)^2}, \tag{9}$$

where N is the total number of points in each segment. The distribution of the rms prediction error in the i, j plane will then indicate which segments have similar dynamics and thus predict each other well by yielding a minimum error.

Application to the tremor data

The cross-prediction method described above was applied to the tremor data in order to investigate the possibility of temporal variations of phase space dynamics. An analysis window of 20 min was chosen again, with a length for each segment of 1 min (1200 samples). In practice the selection of the segment length should be determined in such a way that enough points will be available for a reliable estimate of $\gamma(i, j)$ without making the segments unnecessarily long, which may result in degrading the time resolution of the prediction error distribution. The initial neighbourhood size ϵ was taken as the variance of the samples in the analysis window divided by 1000 and a minimum number of 30 neighbours was required in order to make each prediction. If the neighbours found were less

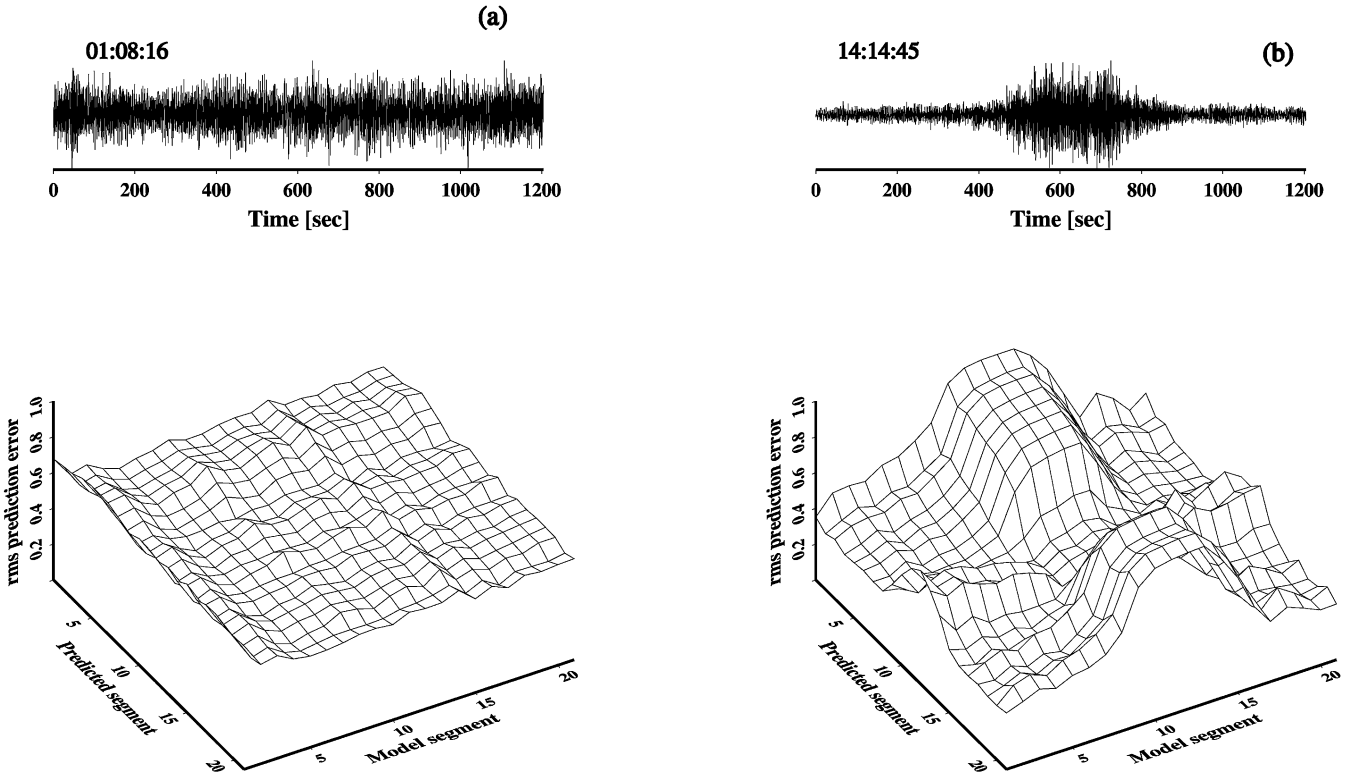

Figure 12. Distribution of the rms prediction error versus model and predicted data segments for (a) continuous tremor, (b) cigar-shaped bursts and low-amplitude background tremor recorded on October 1. The times given on the right are the start times (GMT) for each trace.

than 30, the neighbourhood size increased by a factor of 1.2 until the minimum number was reached. The embedding parameters were those determined earlier, i.e $\tau = 1$ and $m = 7$–8.

The analysis revealed two different patterns of the distributions of the rms prediction error, each being correlated to the tremor activity seen on the seismograms. For the continuous tremor recorded during the early hours of October 1 the prediction error shows an almost flat surface in the (i, j) plane (Fig. 12a), indicating similar dynamics throughout the 20 min of the analysis window. This changes dramatically when the cigar-shaped bursts start appearing superposed on the background tremor. The prediction error surface becomes distorted and the segments that correspond to the bursts can only predict themselves well forming a minimum, giving a maximum error when they are used to predict the segments of the background tremor (Fig. 12b). In cases when there was more than one burst in the analysis window, it was found that the segments corresponding to one burst could equally well predict the segments of the other, indicating again a similarity of phase space dynamics. The difference in the dynamics of cigar-shaped bursts and background tremor was also found to have an effect on their amplitude spectra. The spectra of the bursts and of high-amplitude continuous tremor exhibit an almost exponential decay at high frequencies in contrast to the low-amplitude background tremor spectra that have a power-law decay. An exponential decay of the amplitude spectrum has also been found as a characteristic of signals generated by low-dimensional chaotic processes (Sigeti & Horsthemke 1987).

DISCUSSION AND CONCLUSIONS

The suggestion that volcanic tremor is the result of non-linear source processes involving one or several different kinds of magmatic activity is not only supported by theoretical considerations (Shaw 1992; Julian 1994), but also by certain characteristics observed in tremor signals, which are believed to be common among systems exhibiting aperiodic, chaotic behaviour. Such characteristics have also been found in the tremor that accompanied the 1996 Vatnajökull eruption in central Iceland and include:

(i) autocorrelation functions that rapidly reach zero;

(ii) broad-band spectra that decay exponentially in higher frequencies; and

(iii) the existence of an attractor, a fractal geometrical object, formed by orbits that move within a bounded region of a low-dimensional Euclidean space, describing the evolution of the states of the system that generates tremor.

In an earlier study, Chouet & Shaw (1991) investigated the possibility that volcanic tremor occurring at Puu Oo crater, Hawaii, was generated by a non-linear source exhibiting chaotic behaviour. Visual observations of the volcanic activity near the crater indicated that the tremor recorded on the seismograms was the result of complex processes of magma flow and degassing operating over a hierarchy of scales. Having recorded the tremor activity at a rate of 200 samples s^{-1} they were able to recover the attractor describing the tremor source, which had a disc-shaped structure strikingly similar to the attractor shown in Figs 8(a) and (b). The calculation of its fractal dimension at different stations for sliding windows of 10 s showed that it was fluctuating in the range of 3.1–4.1 with a mean of 3.75. Owing to the presence of noise superposed on the tremor signal, the authors considered these values to represent the upper bounds of the attractor dimension. The fact that these dimension values were low was interpreted as an indication that the tremor dynamics 'oscillate' between a stable, quasi-periodic and a chaotic regime.

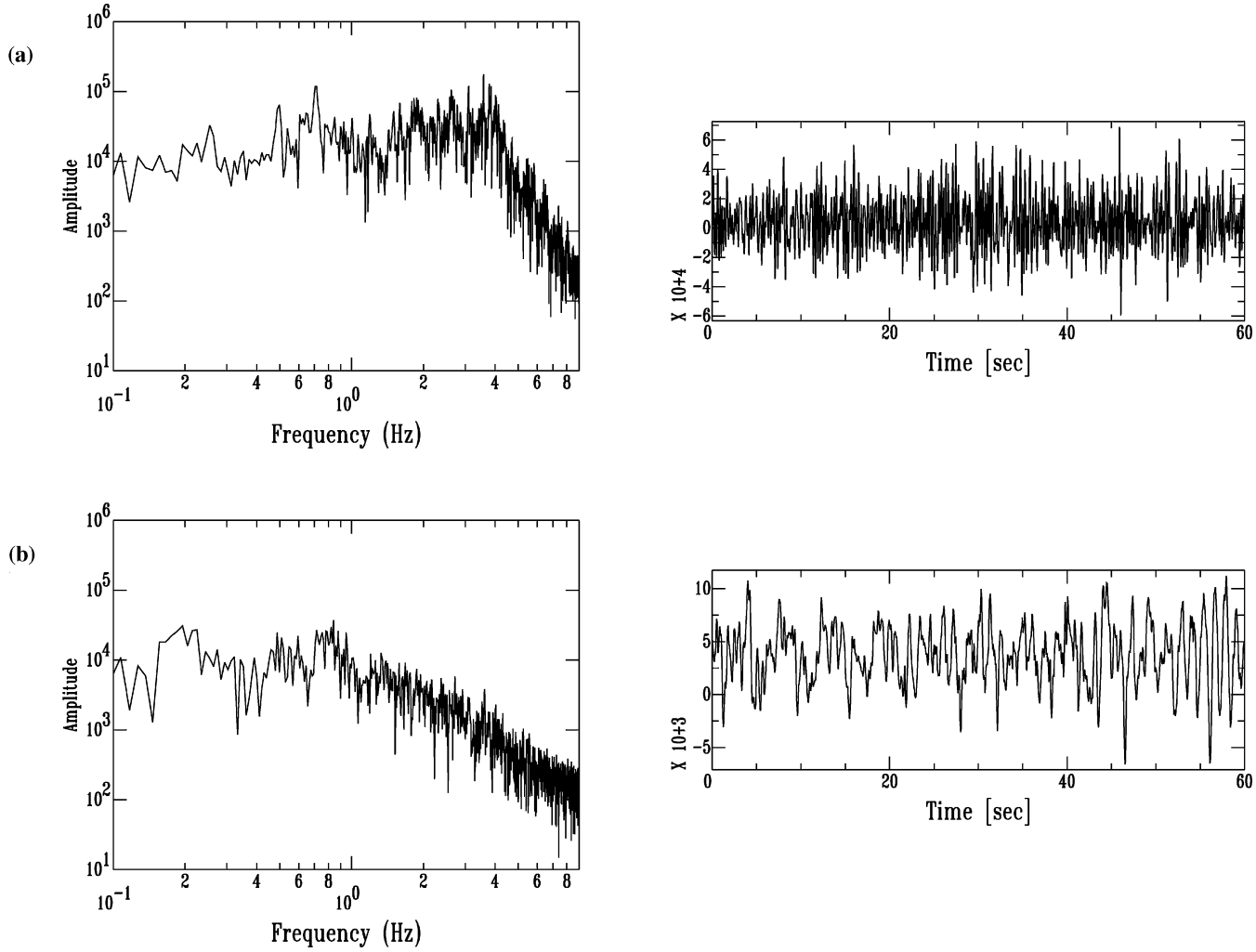

Figure 13. Log_{10}–log_{10} graphs of the amplitude spectrum and corresponding waveforms for 1 min of (a) a high-amplitude burst and (b) low-amplitude background tremor. Note the different rate of decay in the high frequencies and the higher-frequency content of the burst.

The similarities between the properties of the Vatnajökull and Hawaiian tremor as demonstrated by the appearance of the attractors and the upper bounds of their fractal dimensions, point to the possibility of universal characteristics of tremor source processes. Furthermore, the conclusion of Chouet & Shaw (1991) of a tremor process that operates between two different regimes, agrees well with the results obtained by the cross-prediction method. Tremor starts continuously at the beginning of the eruption, exhibiting chaotic behaviour and later evolves to a stable, quasi-periodic signal interrupted by large-amplitude, chaotic bursts. This phenomenon has been observed in other non-linear systems, such as experiments on Rayleigh–Bénard thermal convection in a fluid (Bergé *et al.* 1980) or in the theoretical model of atmospheric flow formulated by Lorenz (Manneville & Pomeau 1980) and has been termed 'intermittency'. Laboratory experiments have shown that the intermittent regime usually occurs when a control parameter (e.g. the Reynolds number) has reached a critical value.

The identification of the physical mechanism causing the tremor observed during the Vatnajökull eruption, however, is still subject to uncertainty. A possible model that can be derived from the observations presented above, may have to do with two different magma flow regimes, one generating continuous tremor and the other background tremor interrupted by bursts. Intermittent turbulence owing to the transition from a purely laminar to a turbulent flow may be a good candidate for explaining the excitation of Vatnajökull tremor. Assuming that the magma reservoir is connected to the surface with a narrow cylindrical conduit of length l and diameter d (where $l/d > 50$), then as the Reynolds number increases owing to an increase in the flow velocity, turbulent slugs may develop and ascend through the conduit (Faber 1995). The slugs will be separated from each other by intervals of laminar flow and will exert a variable force on the conduit walls. Continuous tremor, therefore, may be the result of ascending turbulent slugs separated by small intervals of laminar flow. As time elapses and the Reynolds number decreases these intervals become larger, giving rise to background tremor, while the slugs generate the observed bursts. Turbulent slug flow of hydrothermal fluids and gases has been used by Hellweg (2000) as one possible explanation for harmonic tremor occurring during a non-eruptive period at Lascar volcano, Chile.

A very important aspect stemming from the observed low-dimensional nature of the tremor signals, is that it may be possible to describe the tremor source using just a small number of ordinary, rather than partial differential equations, which arises as a

consequence of the small number of degrees of freedom involved (Procaccia 1988). Future studies should try to formulate such a mathematical model of the interactions between the fluid flow and the conduit walls, which can reproduce the observed behaviour of tremor signals qualitatively.

ACKNOWLEDGMENTS

I would like to thank the members of the HOTSPOT group: G. Nolet, W.J. Morgan, R.M. Allen, M.J. Pritchard, G.R. Foulger, B.R. Julian, R. Stefánsson, S. Jakobsdóttir, K. Vogfjörd, P. Erlendsson, S. Ragnarsson and B. Bergsson. Neil Goulty, Christine Peirce and two anonymous reviewers provided many helpful comments that improved this manuscript. The HOTSPOT project was funded by the National Environmental and Research Council (NERC) grants GST/02/1238 and GR3/10727 held by G.R. Foulger, NSF grant EAR 9417918 and supported by the US Geological Survey. IRIS/PASSCAL offered technical support and assistance in running the network. The TISEAN software package (Hegger *et al.* 1999) was used for non-linear time-series analysis of the data. All the maps and diagrams were plotted using the GMT software package (Wessel & Smith 1995), and the figures containing waveforms and spectra were produced using SAC2000 (Goldstein *et al.* 1998).

REFERENCES

Abarbanel, H.D.I., 1996. *Analysis of Observed Chaotic Data,* Springer, New York, 272 pp.

Abarbanel, H.D.I., Brown, R., Sidorowich, J.J. & Tsimring, L.S., 1993. The analysis of observed chaotic data in physical systems, *Rev. Mod. Phys.,* **65,** 1331–1392.

Bergé, P., Dubois, M., Manneville, P. & Pomeau, Y., 1980. Intermittency in Rayleigh–Bénard convection, *J. Phys. Lett.,* **41,** L341–L345.

Brandstätter, A. & Swinney, H.L., 1987. Strange attractors in weakly turbulent Couette–Taylor flow, *Phys. Rev. A,* **35,** 2207–2220.

Chouet, B., 1985. Excitation of a buried magmatic pipe: a seismic source model for volcanic tremor, *J. geophys. Res.,* **90,** 1881–1893.

Chouet, B., 1992. A seismic model for the source of long-period events and harmonic tremor, in *Volcanic Seismology, IAVCEI Proceedings in Volcanology,* **3,** 133–156, eds Gasparini, P., Scarpa, R. & Aki, K.

Chouet, B.A. & Shaw, H.R., 1991. Fractal properties of tremor and gas piston events observed at Kilauea volcano, Hawaii, *J. geophys. Res.,* **96**, 10 177–10 189.

Cortini, M., Cilento, L. & Rullo, A., 1991. Vertical ground movements in the Campi Flegrei caldera as a chaotic dynamic phenomenon, *J. Volc. Geotherm. Res.,* **48,** 103–113.

Crosson, R.S. & Bame, D.A., 1985. A spherical source model for low-frequency volcanic earthquakes, *J. geophys. Res.,* **90,** 10 237–10 274.

Drazin, P.G., 1994. *Non-linear Systems,* Cambridge University Press, New York, 317 pp.

Einarsson, P., Brandsdóttir, B., Gudmundsson, M.T. & Björnsson, H., 1997. Center of the Iceland hotspot experiences volcanic unrest, *EOS, Trans. Am. geophys. Un.,* **78,** 374–375.

Faber, T.E., 1995. *Fluid Dynamics for Physicists,* Cambridge University Press, Cambridge, 440 pp.

Ferrazzini, V. & Aki, K., 1992. Preliminary results from a field experiment on volcanic events at Kilauea using an array of digital seismographs, in *Volcanic Seismology, IAVCEI Proceedings in Volcanology,* **3,** 168–189, eds Gasparini, P., Scarpa, R. & Aki, K.

Ferrick, M.G., Qamar, A. & St. Lawrence, W.F., 1982. Source mechanism of volcanic tremor, *J. geophys. Res.,* **87,** 8675–8683.

Fraser, A.M. & Swinney, H.L., 1986. Independent coordinates for strange attractors from mutual information, *Phys. Rev. A,* **33,** 1134–1140.

Frede, V. & Mazzega, P., 1999. Detectability of deterministic non-linear processes in earth rotation time series I. Embedding, *Geophys. J. Int.,* **137,** 551–564.

Fukao, Y., Fujita, E., Hori, S. & Kanjo, K., 1998. Response of a volcanic conduit to step-like change in magma pressure, *Geophys. Res. Lett.,* **25,** 105–108.

Goldstein, P. & Chouet, B., 1994. Array measurements and modelling of sources of shallow volcanic tremor at Kilauea volcano, Hawaii, *J. geophys. Res.,* **99,** 2637–2652.

Goldstein, P., Dodge, D., Firpo, M. & Ruppert, S., 1998. What's new in SAC2000? Enhanced processing and database access, *Seism. Res. Lett.,* **69,** 202–205.

Gudmundsson, M.T. & Björnsson, H., 1991. Eruptions in Grimsvötn, Vatnajökull, Iceland, 1934–1991, *Jökull,* **41,** 21–42.

Gudmundsson, M.T., Sigmundsson, F. & Björnsson, H., 1997. Ice–volcano interaction of the 1996 Gjálp subglacial eruption, Vatnajökull, Iceland, *Nature,* **389,** 954–957.

Hagerty, M.T., Schwartz, S.Y., Garces, M.A. & Protti, M., 2000. Analysis of seismic and acoustic observations at Arenal volcano, Costa Rica, 1995–1997, *J. Volc. Geotherm. Res.,* **101,** 27–65.

Hegger, R., Kantz, H. & Schreiber, T., 1999. Practical implementation of non-linear time series methods: the TISEAN package, *CHAOS,* **9,** 413.

Hellweg, M., 2000. Physical models for the source of Lascar's harmonic tremor, *J. Volc. Geotherm. Res.,* **101,** 183–198.

Jordan, D.W. & Smith, P., 1987. *Non-linear Ordinary Differential Equations,* Oxford University Press, Clarendon, 360 pp.

Julian, B.R., 1994. Volcanic tremor: non-linear excitation by fluid flow, *J. geophys. Res.,* **99,** 11 859–11 877.

Kantz, H. & Schreiber, T., 1996. *Non-linear Time Series Analysis*, Cambridge University Press, Cambridge, 304 pp.

Keers, H., Dahlen, F.A. & Nolet, G., 1997. Chaotic ray behaviour in regional seismology, *Geophys. J. Int.,* **131,** 361–380.

Kennel, M.B. & Isabelle, S., 1992. Methods to distinguish possible chaos from coloured noise and to determine embedding parameters, *Phys. Rev. A,* **46,** 3111.

Kennel, M.B., Brown, R. & Abarbanel, H.D.I., 1992. Determining embedding dimension for phase-space reconstruction using a geometrical construction, *Phys. Rev. A,* **45,** 3403–3411.

Konstantinou, K.I., Nolet, G., Morgan, W.J., Allen, R.M. & Pritchard, M.J., 2000. Seismic phenomena associated with the 1996 Vatnajökull eruption, central Iceland, *J. Volc. Geotherm. Res.,* **102,** 169–187.

Kubotera, A., 1974. Volcanic tremors at Aso volcano, in *Physical Volcanology,* pp. 29–48, eds Civetta, L., Gasparini, P., Luongo, G. & Rapolla, A., Elsevier, Amsterdam.

Leet, R.C., 1988. Saturated and subcooled hydrothermal boiling in groundwater flow channels as a source of harmonic tremor, *J. geophys. Res.,* **93,** 4835–4849.

Li, T.Y. & York, J.A., 1975. Period three implies chaos, *Am. Math. Mon.,* **82,** 985–992.

Lorenz, E.N., 1963. Deterministic non-periodic flow, *J. Atmos. Sci.,* **20,** 130–141.

Lorenz, E.N., 1969. Atmospheric predictability as revealed by naturally occurring analogues, *J. Atmos. Sci.,* **26,** 636.

Manneville, P. & Pomeau, Y., 1980. Different ways to turbulence in dissipative dynamic systems, *Physica D,* **1,** 219–226.

Nettles, M. & Ekström, G., 1998. Faulting mechanism of anomalous earthquakes near Bárdarbunga volcano, Iceland, *J. geophys. Res.,* **103,** 17 973–17 983.

Procaccia, I., 1988. Universal properties of dynamically complex systems: the organisation of chaos, *Nature,* **333,** 618–623.

Ruelle, D. & Takens, F., 1971. On the nature of turbulence, *Commun. Math. Phys.,* **20,** 167–192.

Sauer, T., York, J.A. & Casdagli, M., 1991. Embedology, *J. Stat. Phys.,* **65,** 579.

Schlindwein, V., Wasserman, J. & Scherbaum, F., 1995. Spectral analysis of harmonic tremor signals from Mt Semeru, Indonesia, *Geophys. Res. Lett.,* **22,** 1685–1688.

Schreiber, T., 1997. Detecting and analysing non-stationarity in a time series using non-linear cross-predictions, *Phys. Rev. Lett.,* **78,** 843–846.

Shaw, H.R., 1992. Non-linear dynamics and magmatic periodicity; fractal intermittency and chaotic crises, *Int. Geol. Congr.,* **29,** 510.

Sigeti, D. & Horsthemke, W., 1987. High-frequency power spectra for systems subject to noise, *Phys. Rev. A,* **35,** 2276.

Takens, F., 1981. *Detecting Strange Attractors in Turbulence, Lecture Notes in Math.,* Vol. 898, Springer, New York.

Wessel, P. & Smith, W.H.F., 1995. New version of the generic mapping tools released, *EOS, Trans. Am. geophys. Un.,* **76,** 329.

Zobin, V., 1999. The fault nature of the M_s 5.4 volcanic earthquake preceding the 1996 subglacial eruption of Grimsvötn volcano, Iceland, *J. Volc. Geotherm. Res.,* **92,** 349–358.